

# Far-infrared nebular spectral features from growing massive black holes

Evgenii O. Vasiliev<sup>1,2\*</sup>, Yuri A. Shchekinov<sup>2,3</sup>, Biman B. Nath<sup>3</sup>

<sup>1</sup>*Southern Federal University, Stachki Ave. 194, Rostov-on-Don, 344090 Russia*

<sup>2</sup>*Lebedev Physical Institute of Russian Academy of Sciences, 53 Leninskiy Ave., 119991, Moscow*

<sup>3</sup>*Raman Research Institute, Sadashivanagar, Bengaluru 560080, Karnataka, India*

Accepted 2018 December 32. Received 2018 December 31; in original form 2018 December 31

## ABSTRACT

Supermassive black holes (BHs) and their host galaxies are interlinked by virtue of feedbacks and are thought to be co-eval across the Hubble time. This relation is highlighted by an approximate proportionality between the BH mass  $M_{\bullet}$  and the mass of a stellar bulge  $M_{*}$  of the host galaxy. However, a large spread of the ratio  $M_{\bullet}/M_{*}$  and a considerable excess of BH mass at redshifts  $z \sim 8$ , indicate that the coevolution of central massive BHs and stellar populations in host galaxies may have experienced variations in its intensity. These issues require a robust determination of the relevant masses (BH, stars and gas), which is difficult in the case of distant high-redshift galaxies that are unresolved. In this paper, we seek to identify spectral diagnostics that may tell us about the relative masses of the BH, the gas mass and stellar mass. We consider general features of SEDs of galaxies that harbour growing massive BHs, forming stars and interstellar/circumgalactic gas. We focus on observational manifestations of possible predominances or intermittent variations in evolutionary episodes of growing massive BHs and forming stellar populations. We consider simplified scenarios for star formation and massive BHs growth, and simple models for chemical composition of gas, for dust free gas as well as for gas with dust mass fraction of 1/3 of the metal content. We argue that wideband multi-frequency observations (X-ray to submillimeter) of the composite emission spectra of growing BH, stellar population and nebular emission of interstellar gas are sufficient to infer their masses.

**Key words:** Accretion, accretion discs — black hole physics — *galaxies*: quasars: supermassive black holes — ISM: general — infrared: ISM — submillimeter: ISM

## 1 INTRODUCTION

All massive galaxies in local universe are believed to host supermassive black holes (SMBHs) in their centres. Moreover, the mass of SMBHs  $M_{\bullet}$  are found to correlate with the mass of stellar population  $M_{*}$  of host galaxies (Marconi & Hunt 2003; Häring & Rix 2004; Sani et al. 2011; Kormendy & Ho 2013; Heckman & Best 2014), which suggests a synergy between the formation and growth of SMBHs and their host galaxies. The  $M_{\bullet}$ – $M_{*}$  correlation is however ambiguous. The dominant source of uncertainty stems from measurements of the SMBH mass, because most observational techniques require a calibration of  $M_{\bullet}$  to the observables used to measure it (Bentz et al. 2013; Kormendy & Ho 2013; Woo et al. 2013; Heckman & Best 2014). Further, the determination of stellar mass relies on the ‘mass-to-light’ ratio, which is only known within an ac-

curacy of  $\sim 10\%$  (Kauffmann et al. 2003). For late-type low-mass galaxies ( $M_{*} < 10^{11} M_{\odot}$ ), there can also be uncertainties arising from strong starbursts during the last 1 Gyr (Salim et al. 2005). As a result, the relation between SMBH mass  $M_{\bullet}$  and stellar mass  $M_{*}$  exhibits a spread of more than an order of magnitude (see Fig 9b in Heckman & Best 2014). This has led Heckman & Best (2014) to conclude that the correlation between  $M_{\bullet}$  and  $M_{*}$  in the local universe cannot be approximated as a simple linear proportionality. These complications reflect the nature of mutual feedbacks at work in the process of star formation and a growing SMBH in a host galaxy. At the same time, the analyses by Graham & Scott (2013); Woo et al. (2013) and Kormendy & Ho (2013) indicate that  $M_{\bullet}$  and stellar velocity dispersion in galactic centres  $\sigma$  are coupled tighter than  $M_{\bullet}$ – $M_{*}$ . This implies that black hole growth is regulated mainly by the galaxy gravity, rather than by feedbacks between the growing SMBH and the stellar population, and it

variables in this interplay. However, given the observational uncertainties, it is challenging to disentangle the mutual influences of growing BHs, the assemblage of the host galaxy itself, and the formation of stellar population in it during these epochs.

The problem regarding the  $M_{\bullet} - M_{*}$  relation becomes particularly acute when host galaxies at  $z \simeq 7$  are concerned. Observations of [CII] 158  $\mu\text{m}$  line in a set of  $z \gtrsim 6$  quasars have led Volonteri & Reines (2016) and Decarli et al. (2018) to conclude that the ratio  $M_{\bullet}/M_{*}$  at  $z \simeq 6 - 7$  epochs is more than an order of magnitude higher than that in the local Universe. While at redshifts  $z > 6$ , the mean ratio of the BH to the *dynamical* mass is  $\langle M_{\bullet}/M_{\text{dyn}} \rangle \gtrsim 0.02$  for sufficiently strong ( $S/N \geq 10$ ) [CII] lines (see Fig. 12 in Decarli et al. 2018), at low redshifts  $z \sim 0$  the BH to *stellar* mean mass ratio is only  $\langle M_{\bullet}/M_{*} \rangle \gtrsim 0.003$  when host galaxies with AGNs are concerned (see Fig 10 left in Reines & Volonteri 2015). Under normal circumstances, the ratio of BH mass to dark matter mass would have been smaller in comparison with its ratio to stellar mass. The observed ratios, which are the other way around, perhaps reflect the dynamical features of mutual influences of growing BHs and stellar populations of host galaxies on the initial episodes or during the entire evolution. Examples of such models with  $M_{\bullet}/M_{*}$  up to  $\sim 0.1-1$  are described in Agarwal et al. (2013); Volonteri et al. (2016). However, observational selection effects cannot be neglected in such observations (Decarli et al. 2018), and complementary direct observations would be crucially important for unveiling the synergy between SMBHs and their hosts.

It therefore appears that there may have been periods during the co-eval evolution of SMBH and its host galaxy in which the black hole mass may dominate over stellar and gas mass. It then becomes important to ask if this idea can be tested through observations. Although the masses of BH and stars can be estimated from the spectra of galaxies, such estimates become difficult in the presence of gas and dust. Previous works have identified some spectral features in optical, near- and mid-infrared bands for the case of SMBHs surrounded by interstellar medium of low-metallicity ( $Z \leq 0.05 Z_{\odot}$ ) based on a few scenarios (Agarwal et al. 2013; Natarajan et al. 2017; Volonteri et al. 2017). One scenario implies a  $\sim 100 M_{\odot}$  black hole remnant of a massive Population III star as a SMBH seed (Tanaka & Haiman 2009; Madau et al. 2014; Volonteri et al. 2015; Lupi et al. 2016; Pezzulli et al. 2016), while in the other a more massive direct collapse black hole (DCBH) of  $M \sim 10^5 M_{\odot}$  acts as a seed. In both cases the stellar population is supposed to remain underdeveloped, such that growing BHs dominate the production of photons<sup>1</sup>. Spectral lines in mid-infrared (MIR) range turn out to be sensitive to heating and ionization regimes, which makes them possible in principle to identify with the upcoming *James Webb Space Telescope* (*JWST*). However, scenarios with Pop III black hole seeds predict the MIR line intensities to be weaker than the *JWST* detection limit (Valiante et al. 2016, 2018), which makes it difficult to discriminate between the two scenarios, requiring alternative approaches to be pursued.

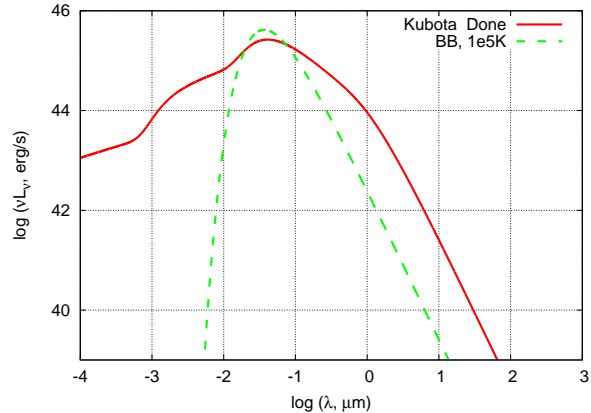


**Figure 1.** Spectral energy distributions for the Kubota & Done (2018) model for  $M_{\bullet} = 10^8 M_{\odot}$  and a black body with  $T = 10^5$  K.

In the current paper we address the question whether observations of spectral energy distributions (SED) consisting of contributions from SMBHs, stellar populations and galactic gas of a distant host galaxy can be disentangled to infer the masses of these three actors. For this purpose we explore the multi-wavelength spectra: X-ray, optical, infrared and far-infrared wavebands to probe the synergy between growing massive BHs and their host galaxies when gas and dust shroud the central BH and stellar population. More specifically, we address the question whether the interrelations between the masses of black hole  $M_{\bullet}$ , of galactic gas  $M_g$ , and galactic stellar population  $M_{*}$  can be inferred through observations of the multi-wavelength spectra from such sources. In order not to increase the number of free parameters, we do not consider an *evolutionary* scenario. We focus only on whether the observed emissions from a galaxy consisting of stars, gas and a supermassive black hole can be discriminated in order to measure the masses of the constituents if the galaxy is not spatially resolved.

The paper is organized as follows. Section 2 contains the model description and numerical setup, Section 3 describes the results, while in Section 4 we discuss observational diagnostics, Section 5 summarizes the results.

## 2 MODEL DESCRIPTION

### 2.1 Spectral energy distribution of a SMBH

Following Natarajan et al. (2017) and Kubota & Done (2018) we assume that SMBH radiation comes from a slim disc (Abramowicz et al. 1988), with the Novikov-Thorne spectrum (Novikov & Thorne 1973) modified by a Comptonised extension up to high ( $E > 1$  keV) energies (see for more detail in Kubota & Done 2018). This choice is motivated by the fact that slim discs are radiatively inefficient and that the accretion flow is stable against Rayleigh-Taylor instability even for super-Eddington accretion rate (see discussion in Abramowicz et al. 1988; Sądowski et al. 2009; Pacucci et al. 2015). An example of the spectrum is shown in Figure 1. For comparison, we also show a blackbody spectrum, which illustrates that in longer wavelengths (infrared

<sup>1</sup> Agarwal et al. (2013) named such stages of galactic evolution

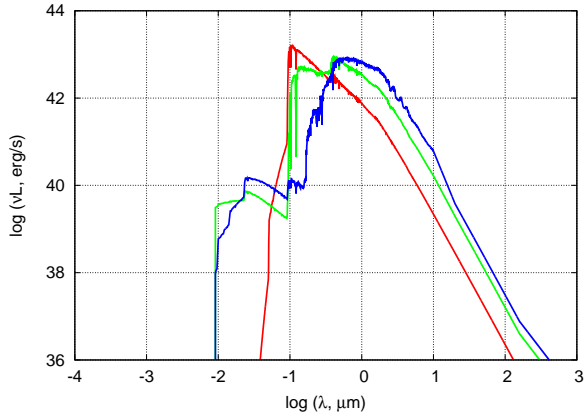


**Figure 2.** Spectral energy distributions for stellar population with ages of 30 Myr for  $[Z/H] = -2$  (red line), of 200 Myr for  $[Z/H] = -1$  (green line) and 1 Gyr for solar metallicity (blue line) (Bruzual & Charlot 2003). The bolometric luminosity is  $L = 3.1 \times 10^9 L_\odot$ .

mal radiation with effective temperature depending on the BH mass  $T_{eff} \propto M_\bullet^{1.5}$  (see Kubota & Done 2018).

## 2.2 Stellar population

For the host galaxy we assume a spectral energy distribution (SED) of a single stellar population (SSP) based on the Padova 2000 stellar evolutionary tracks (Girardi et al. 2000) with the Salpeter initial mass function (IMF) (Bruzual & Charlot 2003). For SSP we consider two models with a low ( $[Z/H] = -2, -1$ ) and with solar metallicity. The bolometric luminosity of the SSP is taken to be  $L = 3.1 \times 10^9 L_\odot$  and  $3.1 \times 10^{10} L_\odot$ , equal to Eddington luminosities of BHs with  $M_\bullet = 10^5 M_\odot$  and  $10^6 M_\odot$ , respectively. The corresponding stellar masses can be roughly estimated as  $M_* \sim 10^{10}$  and  $M_* \sim 10^{11} M_\odot$  for local late-type galaxies (see in Faber & Gallagher 1979).

Figure 2 presents three SEDs models of stellar population from the spectra library of Bruzual & Charlot (2003): a young population of an age 30 Myr for  $[Z/H] = -2$ , a middle-aged (200 Myr) population for  $[Z/H] = -1$  and a moderately old population of 1 Gyr for solar metallicity. Increasing the metallicity for the young SSP leads to an enhanced luminosity at the IR/submm wavelengths. Older populations show two noticeable features in the SEDs. On one hand, in the initial 100 Myr young massive stars dominate in the UV part of the spectrum, and at later epochs, the most massive stars leave the main sequence and evolve into red giants, making the UV part to decline and the infrared emission to rise. On the other hand, low-mass stars at later stages  $\gtrsim 120$ –150 Myr evolve through the post-AGB phase and maintain far-UV emission up to several Gyr.

We are interested in the full spectrum consisting of the cumulative intrinsic spectra of the stars and the SMBH, transmitted through the interstellar gas, and the nebular emission of the ISM ionized and heated by these sources. Our aim is to determine how the spectral features—in the continuum and in lines—in the IR/submm range are connected with the BH and stellar masses, as well as the ISM

connection will allow us to infer a possible correlation between them.

## 2.3 CLOUDY Setup

Ionization states of various elements and the ionic spectral lines are calculated with the CLOUDY code (Ferland et al. 2017). The gaseous layer is exposed to radiation from the central sources, i.e. a BH and stellar population. We assume spherical geometry, in which the inner radius of the layer is fixed at 100 pc, and the outer radius is determined by the gas mass  $M_g$ . The density and metallicity are distributed homogeneously; calculations are done for three gas metallicities:  $[Z/H] = -2, -1$  and 0, corresponding to the stellar population models presented in Figure 2, the fiducial density is  $n = 1 \text{ cm}^{-3}$ . A decrease in the metallicity leads to a nearly proportional decrease of luminosities in metal lines. In runs with gas density different from the fiducial value, the gas mass is kept fixed. We assume that the mass of the layer is fixed, such that the outer radius of the layer varies as  $n^{-1/3}$ . We also assume that the gas is in thermal equilibrium.

## 3 RESULTS

In low-metallicity cases ( $[Z/H] \leq -2$ ), we consider for illustrative purposes a wide range of BH masses  $10^3 \leq M_\bullet \leq 10^8 M_\odot$ . Even though their contribution in heating and ionizing galactic gas in the low BH mass end  $10^3 \leq M_\bullet \leq 10^5 M_\odot$  is not significant (see below in Figure 3), they may reveal anticipated interrelations between emission characteristics of galaxies with BHs at their initial growth episodes. However, when galaxies with higher metallicity are concerned, the effects of interstellar opacity come into play and complicate the calculations. Therefore, in models with high metallicity we limit our calculation to BH masses  $10^5 \leq M_\bullet \leq 10^8 M_\odot$ , because BHs with masses  $M_\bullet \geq 10^5 M_\odot$  are able to ionize absorbing species (carbon, oxygen and nitrogen) in ambient interstellar gas and make it more transparent. Higher gas transmittance also prevents the BHs from producing dynamical (gravitational) feedback effects on the very inner gas and dust layers.

### 3.1 Dust-free gas

Let us first consider the combined effect of the stellar and BH radiation on emissivity of galactic gas with a sub-solar metallicity  $[Z/H] = -2$ . We consider a set of models with a fixed mass of stellar population corresponding to bolometric luminosity  $L_b = 3.1 \times 10^9 L_\odot$ , complemented by radiation from an accreting BH with masses from  $10^3 M_\odot$  to  $10^8 M_\odot$ ; the mass of a surrounding interstellar gas is assumed  $M_g = 10^{10} M_\odot$ . The total radiation from stars and the BH irradiates the diffuse gas, resulting in its ionization, heating and consequently affecting its emissivity.

Figure 3 presents for a low metallicity gas the sum of the stellar and the BH incident flux (*red lines*), the continuum and line emission spectrum from photo-ionized diffuse interstellar gas (*green lines*), and the net transmitted spectrum (*blue lines*). It is seen that, regardless of the low metallicity  $[Z/H] = -2$ , UV and soft X-ray photons produced by

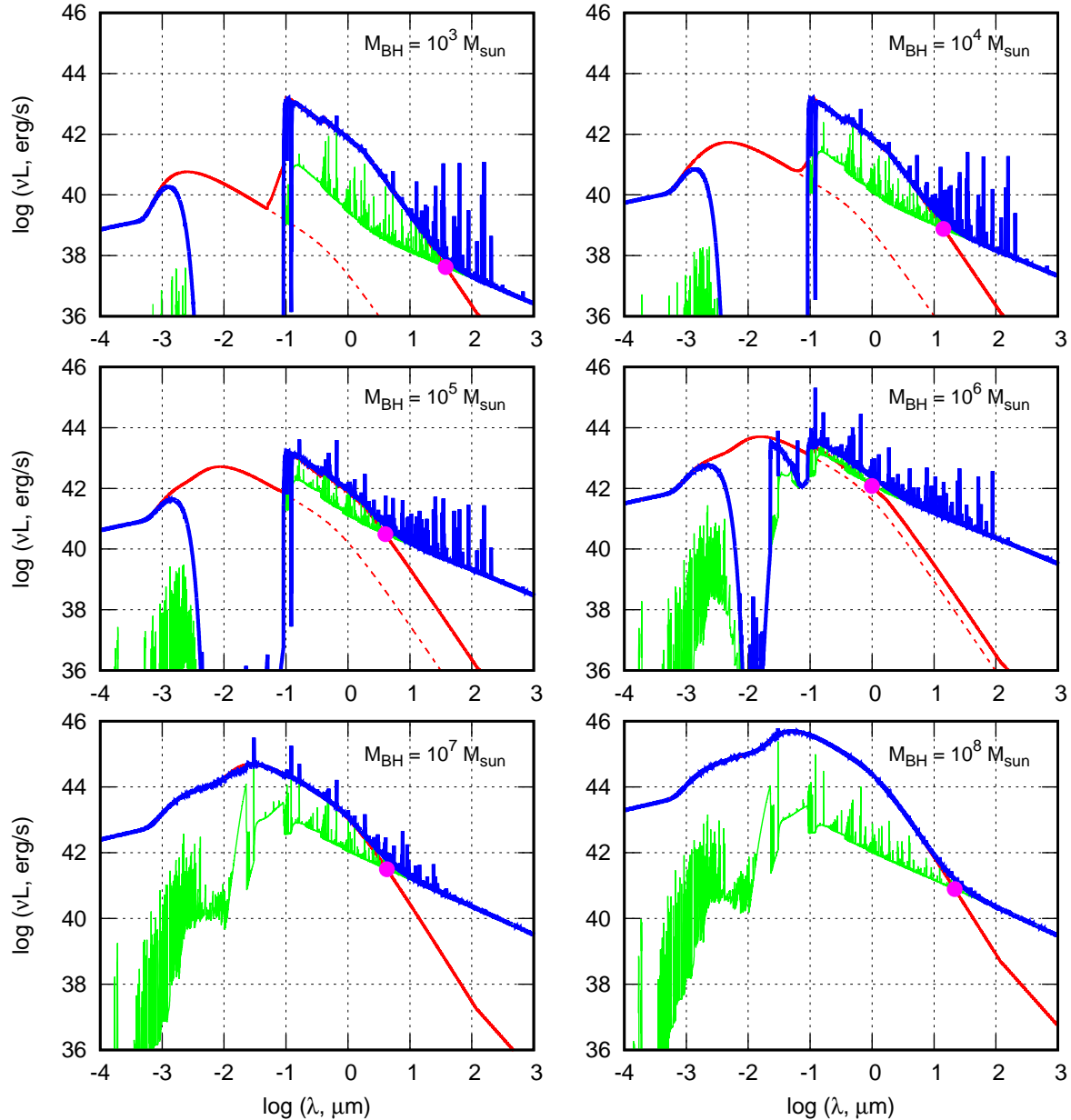


**Figure 3.** Emission spectrum of diffuse interstellar gas photo-ionized by radiation field from a single stellar population and growing BH with mass  $M_{\bullet} = 10^3, 10^4, 10^5, 10^6, 10^7$  and  $10^8 M_{\odot}$ , respectively. The SSP bolometric luminosity is equal to  $L = 3.1 \times 10^9 L_{\odot}$  and the age is 30 Myr, the metallicity is  $[Z/H] = -2$ . The SSP spectrum is presented in Figure 2. A slim-disc spectrum is assumed for the BH (Kubota & Done 2018) with the Eddington bolometric luminosity; gas mass is  $M_g = 10^{10} M_{\odot}$ . Thin red lines depict the sum of stellar plus BH (shown separately by red dashed lines) incident flux, blue lines show the net transmitted spectrum – the sum of an attenuated incident flux plus diffuse continuum and line emission, green lines show the emission spectrum from photo-ionized and heated diffuse interstellar gas. Interstellar density is  $n = 1 \text{ cm}^{-3}$ , gas metallicity  $[Z/H] = -2$ .

fraction of the absorbed energy being converted to IR/sub-mm lines of hydrogen and low ionization states of metals, such as [NII] 121  $\mu\text{m}$ , [CII] 158  $\mu\text{m}$ , [NII] 205  $\mu\text{m}$  and others. However, the most important effect of these photons is an increase in heating and ionization in the gas layer. This manifests in an enhanced free-free nebular continuum.

It is readily seen that gas nebular emission is predominantly due to hard radiation from the BH. As the BH mass increases the nebular luminosity increases proportionally.

this proportionality in continuum emission weakens, while line emission decreases. The corresponding decrease of the neutral fraction makes the outer gas layer more transparent, as can be seen from comparing the mid-left and mid-right panels on Figure 3 for BH mass  $M_{\bullet} \gtrsim 10^5$  to  $M_{\bullet} \gtrsim 10^6 M_{\odot}$ . For higher BH masses (two bottom panels), Hydrogen is completely ionized, and the incident SED remains practically unchanged after passing through the gas layer. Further increase of BH mass above  $M_{\bullet} > 10^6 M_{\odot}$  results in decreasing the ionization of H, H $\alpha$ , and H $\beta$  lines. Note that for

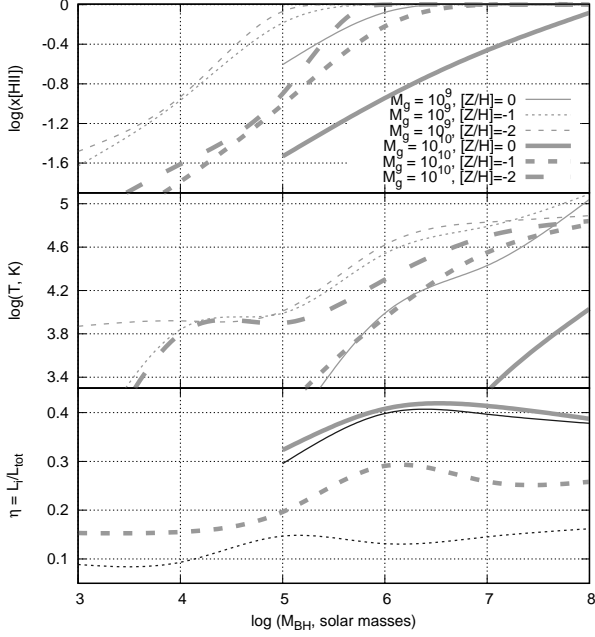


**Figure 4.** HII fraction (*upper panel*), electron temperature (*middle panel*) in gas layer with mass  $M_g = 10^9 M_\odot$  (thin lines),  $10^{10} M_\odot$  (thick lines) and metallicity  $[Z/H] = -2$  (dashed lines),  $-1$  (dotted lines),  $0$  (solid lines) exposed to the radiation field from a SSP with bolometric luminosity equal to  $L_* = 3.1 \times 10^9 L_\odot$  and a growing BH with mass  $M_\bullet$  indicated on  $x$  axis; for  $[Z/H] = -1$  and  $0$  dust is assumed to present with mass fraction  $\mathcal{D} = 0.3\zeta$ . *Lower panel* depicts the fraction of energy spent by stars and BH in heating dust (Sec. 3.2), as shown by thin and thick solid lines, for the gas mass  $M_g = 10^9$  and  $10^{10} M_\odot$  respectively.

same BH mass limit,  $M_\bullet \gtrsim 10^6 M_\odot$ , the BH outshines the stellar radiation from the SSP with bolometric luminosity  $L_* = 3.1 \times 10^9 L_\odot$ .

The luminosity of free-free nebular emission in the IR/submm range increases as  $L_\nu \propto M_\bullet$ , until the BH masses exceeds a critical value  $M_{\bullet,s}$ , and afterwards it saturates and remains nearly constant at higher  $M_\bullet$ . Assuming that gas in the layer is ionized mostly by EUV and X-ray photons from the BH one can estimate its mass when free-free emission saturates as the BH mass crosses the limit, as follows,

$$M_\bullet > M_{\bullet,s} \sim \frac{\alpha_r n \langle \epsilon_i \rangle M_g}{m_p L_{Edd, M_\odot}} \simeq 10^{-4} n M_g, \quad (1)$$

where  $\alpha_r \simeq 2.3 \times 10^{-13} T_4^{-0.82} \text{ cm}^3 \text{ s}^{-1}$ , the case B hydrogen recombination rate (Draine 2011),  $\langle \epsilon_i \rangle = \int F_\epsilon \sigma_i(\epsilon) \epsilon d\epsilon / \int F_\epsilon \sigma_i(\epsilon) d\epsilon \sim 0.05 \text{ keV}$  is the mean energy of ionized photons,  $F_\epsilon$  is the energy flux of X-ray photons,  $L_{Edd, M_\odot} = 1.26 \times 10^{38} \text{ erg s}^{-1}$  is the Eddington luminosity for a  $M_\bullet = M_\odot$  black hole,  $n$  is gas density in the layer,  $M_g$  is its mass. We assume  $\sigma_i \simeq 2 \times 10^{-22} \epsilon_{\text{keV}}^{-2.5} \text{ cm}^2$  for H + He plasma (Wilms et al. 2000).

For a gas mass of  $M_g = 10^{10} M_\odot$  Eq. (1) gives  $M_\bullet \sim 10^6 M_\odot$ . The fractional ionization  $x \lesssim 1$ , as seen in Figure 4 and further growth of  $M_\bullet$  does not increase the luminosity of nebular emission. Assuming for H + He plasma the cooling rate  $\Lambda_{\text{neb}} \simeq 3 \times 10^{-25} T_4^{1/2} \text{ erg cm}^3 \text{ s}^{-1}$  – the sum of free-free

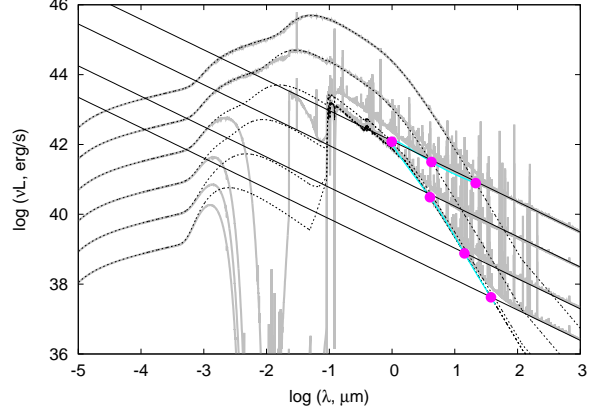


**Figure 5.** A schematic presentation of the spectra shown in Figure 3 (all transmitted spectra in one plate, the emission spectra from photo-ionized diffuse interstellar gas are replaced by lines with slopes followed by the free-free continuum). The thick dark grey line depicts the SSP incident spectrum. The set of thick light grey lines present the total transmitted spectra for the SSP+BH source. The straight thin lines follow pure free-free continuum. Color symbols depict the location of intersection points.

the fraction of bolometric BH luminosity being radiated as nebular emission,

$$\eta_{\text{neb}} \sim 3 \times 10^{-6} x^2 n T_4^{1/2} \frac{M_g}{M_\bullet}. \quad (2)$$

For  $M_\bullet = 10^6$ , this fraction is  $\eta_{\text{neb}} \sim 0.3$  for fiducial parameters, and it decreases with an increase in  $M_\bullet$ .

In the long-wavelength limit, the free-free nebular spectral luminosity  $L_\nu^n \propto \nu^{-0.12} \propto \lambda^{0.12}$ . This scaling is shallower than that of the sum of stellar and BH spectra,  $L_\nu^{\text{SSP+BH}} \propto \nu^2 \propto \lambda^{-2}$ . Therefore, at a certain wavelength  $\lambda_i$ , the nebular emission outshines the radiation from the original sources. At  $\lambda_i$ , the net transmitted spectrum changes from the slope  $\alpha = -2$  shortward to  $\alpha = -0.12$  longward. In Figure 3, we show the spectra in the form of  $\mathcal{L}_\nu \equiv \nu L_\nu$ , which changes from  $\mathcal{L}_\nu \propto \nu^3 \propto \lambda^{-3}$  in the short-wavelength side  $\lambda < \lambda_i$  to  $\mathcal{L}_\nu \propto \nu^{0.88} \propto \lambda^{-0.88}$  after the inflection point, located in the far-IR or the sub-mm wavelength range depending on masses of SPP, BH and the ambient gas layer. The presence of such an inflection point in spectrum of a distant source would indicate the prevalence of the nebular emission.

Magenta points in Figure 3 depict the intersection between the free-free continuum and stellar/BH thermal background. One can observe that for a given SSP luminosity an increase of BH mass leads to a shift of the intersection towards shorter wavelengths with simultaneous increase of the luminosity, until the SSP dominates in the optical and IR range – it is seen in the four upper panels of Figure 3, for BH masses from  $10^3$  to  $10^6 M_\odot$ . For more massive and brighter BHs the free-free continuum saturates and further increase of the BH mass shifts the inflection point to longer wavelengths with simultaneous decrease of luminosity.

For clarity, we collect all spectra in a schematic plot on Figure 5. The thick dark grey line depicts the SSP incident spectrum. A set of thick light grey lines presents the total transmitted spectra of SSP+BH source with increasing val-

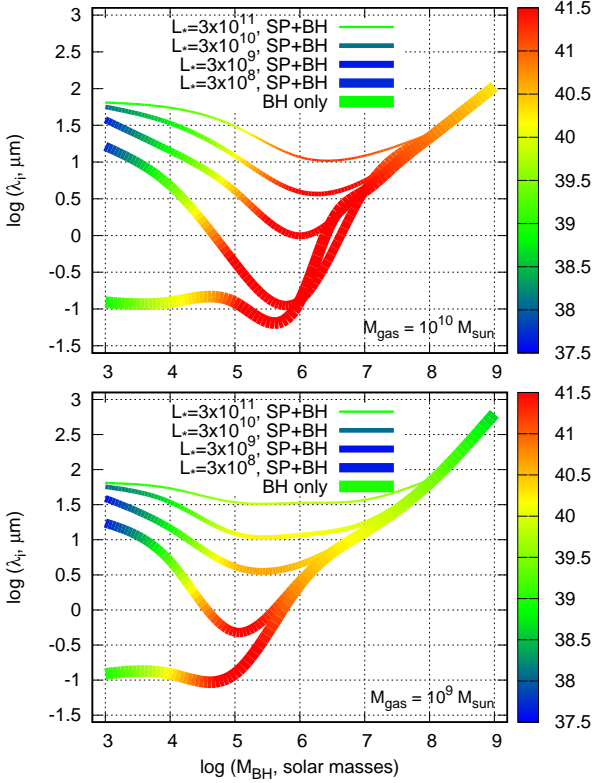


**Figure 6.** The wavelength of the intersection (magenta points in Figure 3) between the free-free continuum by the photoionized gas and the net transmitted spectrum – the sum of an attenuated incident flux plus diffuse continuum and line emission versus the BH mass for four values of stellar population luminosity: no stellar population (the thickest line, ‘BH only’),  $L_* = 3.1 \times 10^8$ ,  $3.1 \times 10^9$ ,  $3.1 \times 10^{10}$ ,  $3.1 \times 10^{11} L_\odot$  (from thicker to thinner lines). The SSP age is 30 Myr. The gaseous mass of the layer exposed to the radiation is  $M_g = 10^{10} M_\odot$  (upper panel),  $10^9 M_\odot$  (lower panel). The color along the lines correspond the logarithm of luminosity  $\nu L_\nu$  reached at the intersection point.

tinuum. Colour symbols depict the location of intersection points. One can note that there is a turning point for the BH mass value  $M_\bullet \sim 10^6 M_\odot$ , when the free-free emission saturates. Another representation of such loop-like behaviour of the inflection wavelength on the mass of an illuminating BH is given in Figure 6.

The colours on lines in this figure correspond to the luminosity  $\mathcal{L}_\nu$  at the inflection point as coded in the colour bar. The BH mass is a two-valued function of  $\lambda_i$  and the luminosity  $\mathcal{L}_\nu$ . The dropping branch of  $\lambda_i(M_\bullet)$  reflects that SPP optical and IR emission outshines the BH emission. On the right hand side of the Figure,  $\lambda_i(M_\bullet)$  turns to grow when this relation reverses, approximately at  $M_\bullet > M_{\bullet,s}$ .

### 3.1.1 Spectral lines

Nebular spectral emission is fed by both UV from stars and by X-ray and UV from the growing black hole. As mentioned above, the contribution from young stellar population (SSP) is restricted by a very narrow UV band  $\lambda = 500\text{--}1000\text{\AA}$  from OB stars. As a result, in optical and near infrared range,

ion remains weak. This is clearly seen in Figure 3: when the BH mass lies within  $M_\bullet < 10^5 M_\odot$  all optical and even a fraction far IR nebular lines fall below the stellar emission. Only from  $M_\bullet \geq 10^5 M_\odot$  onward, the nebular lines emerge over and above the stellar continuum due to a predominant contribution of the BH towards ionization. However, further increase of the BH mass  $M_\bullet > 10^6 M_\odot$  results in a higher ionization and in a suppressed hydrogen recombination optical emission. Ultimately at  $M_\bullet \geq 10^7 M_\odot$  nebular emission becomes saturated.

We illustrate this in Figure 7 where relative intensities of nebular emission lines  $\mathcal{F}_\lambda = (F_l(\lambda) - F_c)/F_c$ , are shown against the black hole X-ray luminosity in the 0.1–3 keV energy band. Here  $F_l(\lambda)$  is the line-centre intensity,  $F_c$  is the net continuum intensity on both sides of the line. The upper row shows the dependences of relative line intensities when the gas layer is illuminated only by a BH with different masses. From left to right, optical hydrogen recombination lines  $H\alpha$ ,  $H\beta$  and  $B\alpha$ , mid- and far-IR high ionization ions lines: [MgVII] 5.5, 9  $\mu\text{m}$ , [NeVI] 7.6  $\mu\text{m}$ , and [NeV] 24  $\mu\text{m}$ , [NIII] 57  $\mu\text{m}$ , [OIII] 88  $\mu\text{m}$  respectively, in middle column panels, and far-IR lines of neutrals and low-ionization species: [SiII] 34  $\mu\text{m}$ , [OI] 63  $\mu\text{m}$ , [NII] 121  $\mu\text{m}$ , [OI] 145  $\mu\text{m}$ , [CII] 158  $\mu\text{m}$  in the right column panels, are presented. All lines with similar behaviour are joined by grey shade in order to clearly illustrate their similarity. It is readily seen that when the gas is illuminated only by a BH, the Hydrogen lines do not show an increase in intensity with increasing BH mass until  $M_\bullet \lesssim 3 \times 10^6 M_\odot$  (corresponding to  $L_x \lesssim 10^{42} \text{ erg s}^{-1}$ ). Nearly the same dependence is shown by [NeV], [NIII], [OIII] in middle column panel. Intensities of ions with mid-IR lines [MgVII] and [NeVI] reveal a gradual growth with the BH mass ( $\mathcal{F}_\lambda \propto M_\bullet^{1/3}$ ) for  $M_\bullet \lesssim 3 \times 10^6 M_\odot$ . In contrast, far-IR lines of low ionization and neutral species: [SiII], [OI], [NII], [OI], [CII] (right panel) drop quickly, as  $\mathcal{F}_\lambda \propto M_\bullet^{4/3}$ , and practically disappear at  $M_\bullet \gtrsim 3 \times 10^6 M_\odot$ .

The second row in Figure 7 demonstrates the changes in line intensities, when irradiated by a young (30 Myr) SSP with the luminosity  $L_* = 3 \times 10^9 L_\odot$  (the equivalent mass is  $M_* \simeq 10^{10} M_\odot$  for a Salpeter IMF). Being strongly suppressed by stellar continuum in  $\lambda = 0.1\text{--}1 \mu\text{m}$  range, the relative intensities of nebular optical lines drop by two orders of magnitude in the low end of the BH X-ray luminosity. The decrease factor remains nearly constant when the SSP luminosity grows:  $L = 3 \times 10^{10} L_\odot$  (third panel from top, left column), and  $= 3 \times 10^{11} L_\odot$  (lowest panel, left column). This approximate constancy stems from the fact that while the BH with masses  $M_\bullet \lesssim 10^5 M_\odot$  contributes less towards nebular luminosity in  $\lambda \sim 0.1\text{--}5 \mu\text{m}$  than the stellar continuum, the nebular emission grows nearly proportionally with stellar luminosity. The intensities of optical lines grow with the BH mass, (nearly  $\propto M_\bullet^\alpha$ , with  $\alpha \approx \frac{1}{2}\text{--}\frac{1}{3}$ ), for  $M_\bullet \leq 3 \times 10^6 M_\odot$  for  $L_* = 3 \times 10^{10}$  and  $= 3 \times 10^{11} L_\odot$ , respectively.

Mid-IR lines (dark grey shades) in the middle column panels show a behaviour similar to the optical ( $H\alpha$ ,  $H\beta$  and  $B\alpha$ ) lines, though with a noticeable steepening of growth  $\mathcal{F}_\lambda(M_\bullet) \propto M_\bullet^\alpha$  with  $\alpha \sim 1/3, 2/3, 1$  from SSP luminosity  $L_* = 3 \times 10^9$  to  $L_* = 3 \times 10^{11} M_\odot$ , correspondingly. Far-IR lines of high ionization species (light-dark shades) in the middle columns show a rather weak dependence on BH mass

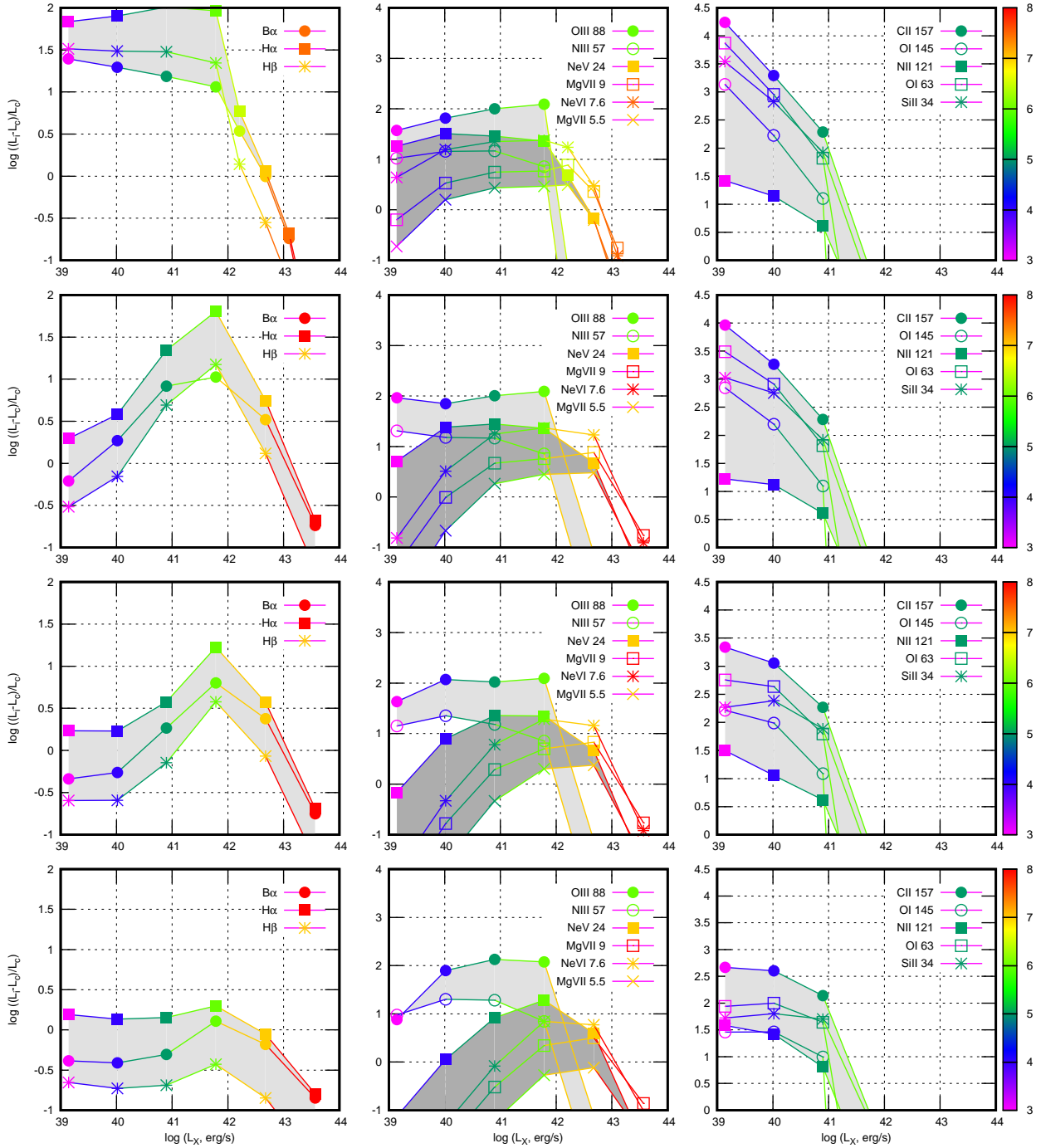


**Figure 7.** Relative intensities of different emission lines shown versus the black hole X-ray luminosity in the 0.1–3 keV band: *left* column depicts hydrogen recombination lines ( $H\alpha$ ,  $H\beta$  and  $B\alpha$ ), *middle* column shows Mid IR and IR lines of highly charged ions, and *right* column shows far IR lines of neutrals and singly charged ions. Panels from top downward depict relative intensities for gas illuminated only by a central black hole (*upper* row), SSP with  $L_* = 3 \times 10^9 L_\odot$ , with  $L_* = 3 \times 10^{10} L_\odot$ , and with  $L_* = 3 \times 10^{11} L_\odot$ , correspondingly; gas mass in all panels is  $M_g = 10^{10} M_\odot$ . The color bar marks logarithmic values of black hole masses corresponding to the Eddington luminosity.

SSP luminosities, from upper to lower rows of panels. Given this ‘conservative’ trend, the ratios of intensities of hydrogen optical lines, mid-IR lines of the ions [MgVII] and [NeVI] as well as of far-IR lines of low ionization and neutral species to the lines of [NIII] and [OIII] can serve to measure the ratio

of the BH mass (luminosity) to the young SSP luminosity within the range shown in Figure 7 (for  $M_\bullet \lesssim 3 \times 10^6 M_\odot$ ).

The ratios of intensities between the lines from the three bands – optical, mid-IR and far-IR/submm to [NIII]  $57\mu\text{m}$  – versus the BH mass are presented in Figure 8,

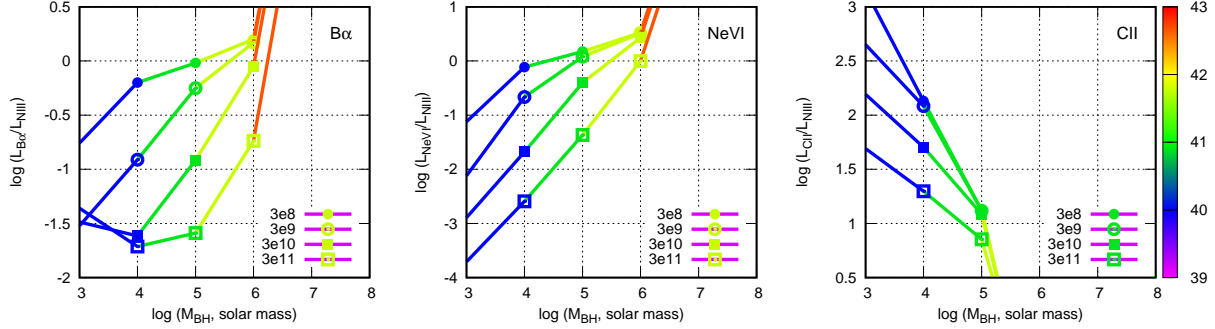


**Figure 8.** The line ratios – relative intensities of the lines  $B\alpha$ ,  $[\text{NeVI}]$  and  $[\text{CIV}]$  to the intensity of the line  $[\text{NIII}]$  – left to right shown versus the BH mass, for different luminosities of the stellar population from  $L_* = 3 \times 10^8 L_\odot$  to  $3 \times 10^{11} L_\odot$  as legended. Lines are color-coded according to the BH X-ray luminosity according to the color bars.

$10^8 L_\odot$  to  $3 \times 10^{11} L_\odot$ . The relative intensities of  $[\text{B}\alpha/\text{NIII}]$ ,  $[\text{NeVI}/\text{NIII}]$  and  $[\text{CIV}/\text{NIII}]$  vary in a wide range spanning more than two orders of magnitude, with  $[\text{B}\alpha/\text{NIII}]$  and  $[\text{NeVI}/\text{NIII}]$  growing from  $\sim 0.03$  to  $\sim 3$  when BH mass increases from  $\sim 10^3$ – $10^4 M_\odot$  to  $\sim 2 \times 10^6 M_\odot$ , depending on the SSP luminosity. At the same time,  $[\text{CIV}/\text{NIII}]$  drops from  $\sim 10^{1.5}$ – $10^{2.7}$  to  $< 3$  in the same range. Note that the line ratios are not single-valued functions of the  $M_\bullet$  to  $M_*$  ratio.

As seen from Figure 7, for  $M_\bullet \gtrsim 3 \times 10^6 M_\odot$  all line intensities decrease steeply because of a growing contribution of the BH beyond the optical band. Another consequence is that BHs with masses in this range outshine stellar light even with  $L_* \sim 3 \times 10^{11} L_\odot$ , so that stellar population becomes difficult to identify. Only the submm continuum nebular emission becomes the sole carrier of information about the ionized gas, as shown in the right column of Figure 6.

The results discussed above and illustrated in Figures 7 and 8 weakly depend on gas mass, and therefore the intensity ratios  $[\text{B}\alpha/\text{NIII}]$ ,  $[\text{NeVI}/\text{NIII}]$  and  $[\text{CIV}/\text{NIII}]$  can serve as direct measures of masses of the stellar population and the BH feeding the nebular line emissions, unless the BH mass exceeds  $M_\bullet \sim 3 \times 10^6 M_\odot$ . The results however change with gas metallicity: the line intensities of heavy elements grow approximately linearly with metallicity ( $\mathcal{F}_\lambda \propto Z$ ) as shown in Figure A1 in Appendix A. The intensities of Hydrogen recombination lines slightly decrease with metallicity as  $\propto Z^{-1/4}$  because of a decrease in the recombination rates due to a metal enhanced radiative cooling (see left column in Figure A1). This results in a nearly proportional increase in the intensity ratio  $[\text{B}\alpha/\text{NIII}]$  with  $Z$  at given  $M_\bullet$  and  $M_*$ , leaving the ratios  $[\text{NeVI}/\text{NIII}]$  and  $[\text{CIV}/\text{NIII}]$  unchanged.

### 3.2 Signatures of stellar and BH in thermal dust emission

As seen in Sec. 3.1.1, the presence of metals in the gas layer clearly manifests itself in a characteristic line spectrum, with line intensities proportional to the metallicity, which can be a useful tool as a diagnostic of the mutual evolution of growing black holes and stellar evolution in a host galaxy, unless dust overwhelms in optical/UV extinction and thermal IR

However, the presence of dust particles in the interstellar gas complicates the picture. Assuming a Milky Way dust extinction law with  $\sigma_v \simeq 5 \times 10^{-22} \zeta \text{ cm}^2$  per H atom (Draine 2011), the extinction depth of the gas layer is  $\tau_v \simeq 7\zeta M_{g,10}^{1/3} n^{2/3}$ , where  $\zeta = Z/Z_\odot$  is a metallicity scaling factor, and  $M_{g,10}$  is the gas mass in our fiducial model in the unit of  $10^{10} M_\odot$ . In the longer wavelength domain up to  $\lambda \lesssim 1000 \mu\text{m}$ , the extinction cross-section decreases as  $\sigma(\lambda) \propto \lambda^{-4/3}$ , for our estimates we assumed the approximation  $\sigma \approx 5 \times 10^{-22} \zeta (\lambda/0.5 \mu\text{m})^{-4/3} \text{ cm}^2$  (see Fig. 5 in Compiègne et al. 2011). As a result, the gas layer becomes transparent,  $\tau(\lambda) \sim 1$ , in the near IR and beyond  $\lambda \sim 2\zeta^{3/4} M_{g,10}^{1/4} n^{1/2} \mu\text{m}$ .

Dust is heated by UV and X-ray radiation from stars and the BH. A considerable fraction of energy absorbed by ambient gas, as seen in Figures 9 and 10, transforms into ionization and heating of the gas and dust. This energy is then partly irradiated in nebular and dust emission. Contribution of the BH dominates gas and dust heating when its mass  $M_\bullet \gtrsim 10^5 M_\odot$  – it is shown by cyan lines in Figures 9 and 10 (which are similar to Figure 3 but for higher metallicity gas, with  $[Z] = -1$  and 0). It is also seen that not only the absolute value of dust emission but even its fraction – the ratio of dust luminosity to the sum of luminosity of stars and BH absorbed in the gas layer – increases with the BH mass, as illustrated in the *lower panel* of Figure 4.

We also find that for  $\zeta \geq 0.1$ , the optical depth  $\tau_{x,uv}$  of the gas volume with radius  $r_h \sim (3M_g/4\pi\rho)^{1/3} \simeq 1.5 \times 10^{22} M_{g,10}^{1/3} n^{-1/3} \text{ cm}$  in X-ray and UV bands exceeds one. Therefore for a rough estimate of dust temperature, one can assume that the most of the heating radiation is absorbed by dust. We also assume the Planck-averaged absorption efficiency  $Q(a, T_d) \simeq \langle Q(a, \nu) \rangle \simeq 0.1 a T_d^2$ , (Dwek & Arendt 1992; Draine 2011), where  $a$  is the grain size in cm, and also that the dust spectral index  $\beta = 2$ :  $Q_\nu(T_d) \propto \nu^\beta$ . With these assumptions the dust temperature is given by

$$T_d \sim 17 \text{ K} (\eta_h \omega)^{1/6} \left( \frac{\langle Q_v \rangle L_{*,9} + \langle Q_x \rangle L_{\bullet,9}}{a_{0.1}} \right)^{1/6} \left( \frac{n}{M_{g,10}} \right)^{1/9} \quad (3)$$

where  $a_{0.1}$  is the dust radius  $a$  in  $0.1 \mu\text{m}$ ,  $L_{*,9}$  and  $L_{\bullet,9}$  are the stellar and black hole luminosities in  $10^9 L_\odot$ ,  $M_{g,10}$  the gas mass in  $10^{10} M_\odot$ ,  $\eta_h = 0.1$ – $0.3$  (see *Lower panel* on Figure 4) is the fraction of energy from the sources – stars and

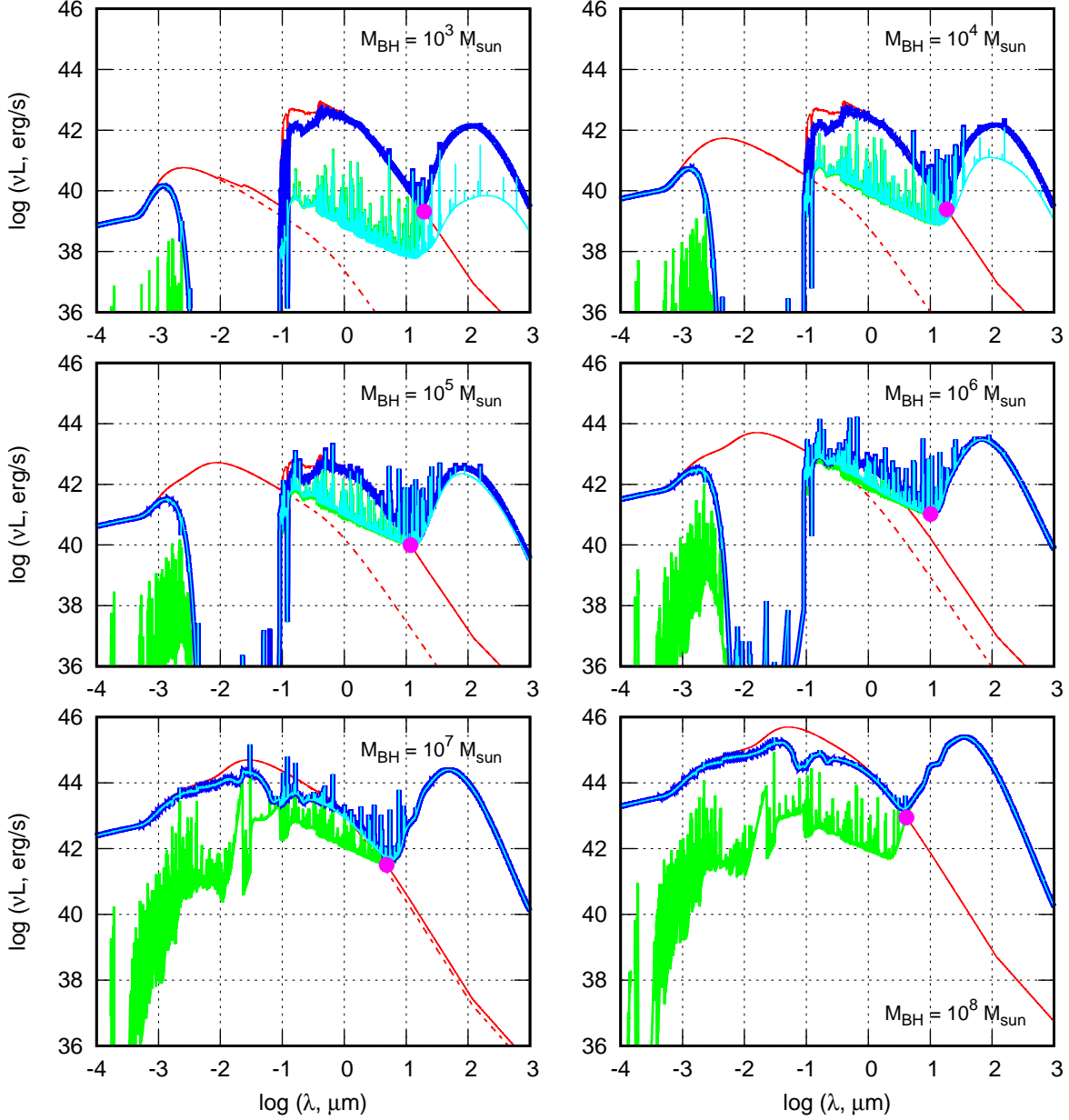


**Figure 9.** Same as in Figure 3 for gas with metallicity  $[Z] = -1$ , and dust with the mass fraction  $\mathcal{D} = 0.3\zeta$ , the stellar population with metallicity  $-1$ , with the luminosity  $L_* = 3.1 \times 10^9 L_\odot$  and the age of 200 Myr is assumed. Cyan lines show the nebular emission under ionization and heating only from the BH.

X-ray and UV photons impinging on the dust grain. In estimates, the absorption efficiencies of dust particles in visual ( $v$ ), EU and X-ray ( $x$ ) bands are assumed to be  $\langle Q_{v,x} \rangle \sim 1$  (see, Fig. 24.1 in Draine 2011). This implies that the characteristic wavelength at the peak dust emission is

$$\lambda_{T_d} \sim 170 \left( \frac{a_{0.1}}{\omega \eta_h \Sigma L_9} \right)^{1/6} \left( \frac{M_{g,10}}{n} \right)^{1/9} \mu\text{m}. \quad (4)$$

with  $\Sigma L_9 = \langle Q_{abs}(v) \rangle L_{*,9} + \langle Q_{abs}(x) \rangle L_{*,9}$ . The estimate is roughly consistent with the peak position in Figure 9.

The  $T_d$  in Eq. (3) is obviously a lower estimate of the dust temperature, whereas in reality, a large fraction of dust

the peak at  $\lambda \sim 70 \mu\text{m}$ . This hot dust is associated with the internal layers with  $\tau_v \sim 7$  for UV and visual photons, and  $\tau_x \sim 3$  for X-ray photons with energy  $\epsilon \sim 1$  keV, where most of heating and ionizing radiation from the stars and the BH is absorbed. This situation is also reflected in a very weak dependence of  $\eta_h$  on the gas mass on *lower panel* of Figure 4. Correspondingly, the peak wavelengths in (4) should be treated as an upper limit of the peak wavelength. This explains the fact that the dust emission in Figure 10 cannot be fit by an isothermal (single temperature) dust. In the left column lowermost panel of Figure 10, we show a modified Planck curve with the emissivity spectral index  $\beta = 2$  and

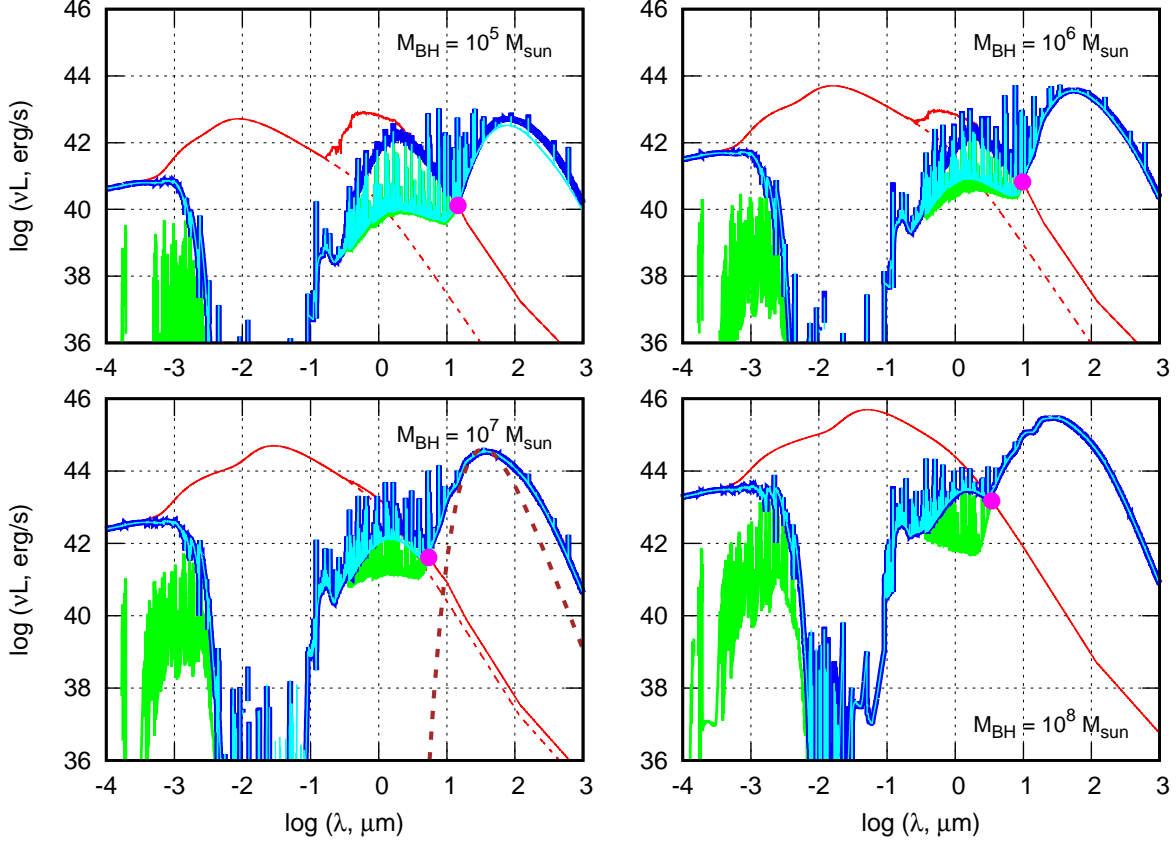


**Figure 10.** Same as in Figure 3 but only  $M_{\bullet} = 10^3$  and  $10^4 M_{\odot}$  for gas with solar metallicity  $[Z]=0$ , and dust with the mass fraction  $\mathcal{D} = 0.3\zeta$ . Cyan lines show the nebular emission under ionization and heating only from the BH. *Brown* dashed line on the lower left panel shows modified blackbody spectra with spectral index  $\beta = 2$  and temperature  $T = 70$  K (see discussion in text). A stellar population has age 1 Gyr and solar metallicity. A worthwhile details can be observed in the upper left panel: the presence of gas results in a decrease of the X-ray emission at  $\lambda \sim 20 \text{ \AA}$ , and an increase of the nebular and dust emission at  $\lambda \gtrsim 10 \mu\text{m}$  – such a reversed reaction in the X-ray high energy band and in FIR/submm range encrypts the interrelation between the masses of BH, gas and dust (discussion in Sec. 4).

line. A deficit of emission (of factor  $\sim 3$  at  $\lambda \sim 100 \mu\text{m}$  to nearly two orders at  $\sim 1000 \mu\text{m}$  in the lower panel) is clearly seen between the modified Planck spectrum and the modeled one, which reflects the negative radial gradient of the dust temperature.

With this stipulation, an upper limit of the dust luminosity can be estimated if one assumes that the fraction  $\eta_h$  of the total (stellar and BH) luminosity heats the *entire* dust mass in the galaxy:  $M_d = \mathcal{D}Z_{\odot}M_g$  with  $\mathcal{D}Z_{\odot}$  being the mass fraction of dust. Assuming the average input rate of heating radiation impinging a dust grain to be  $\sigma\omega\eta_h\Sigma L/4\pi R^2$  and the total number of dust particles in the galaxy  $N_d = M_d/m_d$ , with  $m_d = 4\pi\rho_d/3a^3$ , and  $M_g = 4\pi\rho R^3/3$ , one arrives then at,

$$L_d \sim \eta_h\omega L_9 \frac{\mathcal{D}Z_{\odot}\rho}{4\pi a\rho_d} R, \quad (5)$$

with  $\rho_d = 3 \text{ g cm}^{-3}$  being the dust grain density. For  $\mathcal{D} = 0.3\zeta$ ,  $\zeta = 0.1$ , and  $Z_{\odot} = 0.02$  one arrives at

$$L_d \sim 2 \times 10^{41} \eta_h\omega (L_{*,9} + L_{\bullet,9}) M_{g,10}^{1/3} n^{2/3} \text{ erg s}^{-1}. \quad (6)$$

The contribution from the BH in dust heating obviously prevails when its bolometric luminosity becomes larger than

shown in Figure 9, it occurs when  $M_{\bullet} \gtrsim 10^6 M_{\odot}$ , assuming the critical (Eddington) accretion rate. Beyond this limit information about the stellar population cannot be retrieved from the net spectrum.

At lower masses of BHs  $M_{\bullet} < 10^6 M_{\odot}$ , contributions from BH and stars can be distinguished by making use of the hard X-ray emission of the BH. One can estimate from Figures 3 and 9 that the luminosity in the hard X-ray (energies  $E_X \sim 3 \text{ keV}$ ) varies approximately as  $L_x \propto M_{\bullet}^{4/5}$ . The luminosity of dust emission grows as  $L_{d,p} \propto (M_{*} + M_{\bullet})$ . Combining the observed fluxes of the hard X-ray and the dust peak emission one can infer separately  $M_{*}$  and  $M_{\bullet}$  unless  $M_{\bullet} \gtrsim 10^5 M_{\odot}$ .

More specifically, the two equations connecting the X-ray and thermal dust observables are:  $L_x \simeq 5 \times 10^{36} M_{\bullet}^{4/5} \text{ erg s}^{-1}$  and  $L_d \gtrsim 2 \times 10^{41} (L_{*,9} + 3 \times 10^{-5} M_{\bullet}) \text{ erg s}^{-1}$  as follows from Eq. (6). Here the second term in the parenthesis is the Eddington luminosity  $L_{\text{Edd}} = 1.24 \times 10^{38} M_{\bullet}$  normalized by  $10^9 L_{\odot}$ , and  $M_{\bullet}$  is in  $M_{\odot}$  unit. As a result,

$$M_{\bullet} \simeq 10^5 \left( \frac{L_x}{5 \times 10^{40} \text{ erg s}^{-1}} \right)^{5/4}, \quad (7)$$

$$L_{*,9} \lesssim 28\eta_h^{-1} M_{g,10}^{-1/3} n^{-2/3} L_{d,9} - 7 \left( \frac{L_x}{10^{41} \text{ erg s}^{-1}} \right)^{5/4}. \quad (8)$$

Here the luminosities  $L_d$  and  $L_*$  are normalized by their fiducial values in  $10^9 L_\odot$ . Note that Eq. (8) is valid for  $L_x \leq 2 \times 10^{42} M_{g,10}^{-4/15} n^{-8/15} L_{d,9}^{4/5} \text{ erg s}^{-1}$ , i.e. it is within the limits of the BH contribution in dust heating not exceeding the stellar one, or, equivalently,  $M_\bullet \leq 10^6 M_\odot$ .

### 3.2.1 Spectral lines in a dusty environment

Galaxies with higher stellar and gas metallicities  $[Z/H]=0$  are supposed to be further evolved, and as a consequence, to be more massive, harbouring more massive black holes. In Figure 10 we show the spectra for galaxies with an age of 1 Gyr, stellar luminosity  $L_* = 3.1 \times 10^9 L_\odot$ ,  $M_g = 10^{10} M_\odot$  and metallicity  $[Z/H]=0$ . Panels from left uppermost to right lowermost show cumulative spectra with black holes of masses  $M_\bullet = 10^5, 10^6, 10^7, 10^8 M_\odot$ , respectively.

In a high-metallicity gas spectral lines are obviously more pronounced as compared to those in low-metallicity gas (see Figure A1). However, dust emission floods into the IR/submm range  $\lambda \geq 3\text{--}10 \mu\text{m}$ , and the majority of lines become immersed into the dust emission (Figures 9 and 10). Therefore, in presence of dust, only a few of relatively strong spectral lines in optical and near-IR range are available for  $M_\bullet \gtrsim 10^4 M_\odot$ . For gas metallicity  $[Z/H] = -1$  spectral lines are marginally distinguishable only for black hole masses  $10^5 \leq M_\bullet \leq 10^6 M_\odot$ , and can hardly serve to measure the interrelations between the masses of BH, gas and stellar population. Spectral lines in a gas with higher metallicity are stronger and a few of them remain distinguishable up to  $M_\bullet \sim 10^8 M_\odot$  (Figure 10). These are: [FeII]  $5.3\mu\text{m}$  from regions of low ionization, and [NeVI]  $7.6\mu\text{m}$ , [MgVII]  $5.5\mu\text{m}$ ,  $9\mu\text{m}$  in from high ionization regions. The ratios of their relative luminosities  $\mathcal{L}_{\text{NeVI}} = (L_{\text{NeVI}} - L_c)/L_c$ ,  $\mathcal{L}_{\text{MgVII},5.5} = (L_{\text{MgVII},5.5} - L_c)/L_c$  and  $\mathcal{L}_{\text{MgVII},9} = (L_{\text{MgVII},9} - L_c)/L_c$  vary with  $M_\bullet$  and  $M_g$  and might be utilised to measure them. However, their interrelation becomes degenerate in the higher limit of gas mass  $M_g \gtrsim 3 \times 10^9 M_\odot$ , and in addition does not form a regular sequence along the stellar luminosity.

## 4 DISCUSSION

The main emphasis of the present paper is on finding a method of determining the masses of three important constituents of high redshift galaxies — central supermassive black hole, stars and gas — with the aid of spectral information in X-ray, optical, mid and far infrared wavelengths.

- Observations of very distant ( $z > 6$ ) galaxies hosting growing supermassive black holes provide only their spectra without spatial (angular) structure, and do not allow resolving stellar population and the black hole separately. Therefore, in such conditions, estimates of their masses can only be made from the spectra. However, even though spectral features of relatively young (with the age less than 200 Myr) stellar population are to a certain extent distinguish-

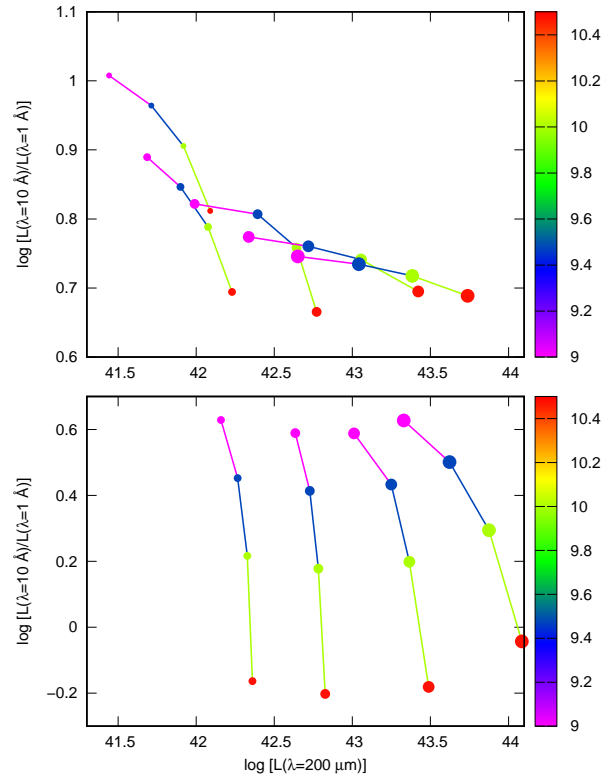


**Figure 11.** Dependence of the ratio of X-ray emission at  $10 \text{ \AA}$  to  $1 \text{ \AA}$  on the sub-mm continuum emission of dust and ionized gas at  $200 \mu\text{m}$  for different masses of the BH: from bottom to top  $10^4, 10^5, 10^6, 10^7, 10^8 M_\odot$ , as indicated by growing sizes of circles; colours show the gas mass in solar units as coded in the colour bar. Upper panel:  $[Z/H]=-1$ , lower panel:  $[Z/H]=0$ . It is seen that in case of lower metallicity the ratio varies with gas mass more weakly than for  $[Z/H]=0$ . The results are shown for fiducial stellar luminosity  $L_* = 3.1 \times 10^9 L_\odot$ ; the dependences  $L(10 \text{ \AA})/L(1 \text{ \AA})$  vs  $L(200 \mu\text{m})$  remain essentially invariant for stellar luminosities  $L_* \lesssim L_{\text{BH}}$ . In case of higher  $L_*$ , the correlations shift to the right, such that at  $L_* = 3 \times 10^{10} L_\odot$  the shift for BH mass  $M_{\text{BH}} \sim 10^5 M_\odot$  ( $L \sim 3 \times 10^9 L_\odot$ ) is around an order of magnitude towards higher emission at  $200 \mu\text{m}$ .

of unknown masses may complicate the situation, thus making a separate determination of masses of stellar population and the hosted SMBH challenging.

- A possible way to overcome this difficulty may involve measurements of emissions that can separately characterize the contributions from the stellar population, the black hole, the gas nebular emission and the dust emission: *i*) high energy X-ray emission  $E \sim 1\text{--}10 \text{ keV}$  can come mostly from the central BH, *ii*) thermal dust emission is supported by heating from the BH and the stars, *iii*) far IR nebular continuum emission in  $\lambda \sim 200 \mu\text{m}$  can give information about the gas mass. With such a multi-wavelength approach, the three observables would provide us with necessary information to infer the three unknowns. Presence of dust complicates such a robust approach and urges additional consideration.

- The role the gas component plays in shaping the cumulative spectrum of a host galaxy bearing a growing black hole is dual: one is that gas absorbs X-ray, UV and optical emission from the BH and stars, the other is that nebular

free continuum in far IR and submm. One can therefore expect that increasing of the gas mass suppresses X-ray and UV/optical light from the sources, and simultaneously enhances nebular emissions. Such a trend is clearly seen in the left upper panel of Figure 10: the solid red line depicts the cumulative spectrum of stars and BH without absorption and emission from gas. As soon as these effects are turned on, they immediately decrease the amount of X-ray and UV photons – the higher the gas mass, the lower is the ionizing photon energy – and of UV/optical/NIR photons in the range from  $\lambda \sim 1000 \text{ \AA}$  to  $\lambda \sim 2 \mu\text{m}$ . The diagram on Figure 11 show such an inverse dependence of an increased of submm free-free  $200 \mu\text{m}$  flux and a decrease of the ratio of X-ray fluxes at  $10 \text{ \AA}$  to  $1 \text{ \AA}$  along with an increasing gas mass.

- This trend can be observed particularly at the high end of BH masses in Figure 11. It is seen that with an increase in the gas mass, the  $200 \mu\text{m}$  flux enhances, with a simultaneous decline of the  $10 \text{ \AA}$  to  $1 \text{ \AA}$  fluxes. Such a concerted anti-correlation of  $200 \mu\text{m}$  and  $10 \text{ \AA}$  to  $1 \text{ \AA}$  fluxes with a growing gas mass can also be seen at smaller BH masses, though becoming flatter with smaller the BH masses. This is because of the fact that the ionizing radiation flux decreases as  $\exp(-\tau_x)$ , where  $\tau_x \propto N_H \propto M_g^{1/3}$  is the optical depth in X-ray/UV (for the assumed parameters  $\tau_x \gtrsim 1$ ), while the  $200 \mu\text{m}$  flux grows as a shallow power-law scaling  $\propto M_g^{1/3}$ .

- In our consideration we explicitly used the black hole spectral energy distribution based on the model described by Kubota & Done (2018), with the X-ray luminosity ( $\epsilon = 0.03\text{--}10 \text{ keV}$ ) scaling as  $L_x \propto M_\bullet^{\alpha}$ . Observationally the interrelation between the X-ray luminosity and the BH mass seems challenging to be robustly inferred, mostly because of contamination from heavy dust obscuration, or lack of direct measures of BH mass when X-ray emission is recognizable (see discussion in Circosta et al. 2019; Connor et al. 2020; Vito et al. 2019; Lambrides et al. 2020; D’Amato et al. 2020). However, our results are qualitatively correct for any positive power-law dependence  $L_x \propto M_\bullet^\alpha$ ,  $\alpha > 0$ , which is obviously the case. Our arguments and resulting interrelations remain largely invariant in this case.

## 5 CONCLUSIONS

We have studied observational manifestations of the interrelation between the masses of stellar population, central massive black hole and the interstellar gas in the host galaxies through their multiwavelength spectral energy distributions from X-ray to submm wavelengths. We modelled cumulative spectra as a sum of emission from growing BHs, stellar populations and nebular emission from interstellar and circumgalactic mass with making use of CLOUDY (version 17). We argue that the three observables: the luminosities (fluxes) in X-ray, dust infrared and submm thermal emission, along with their ratios allow us to infer the masses (luminosities) of the stellar population, the central BH and the gaseous component.

Our results are summarized as follows:

- In dust-free models, emission of growing black holes

free continuum in the far infrared outshines the emission from central source, with a change of spectral shape from a quasi-blackbody spectrum  $\propto \nu^2$  to a flat  $\propto \nu^{-0.12}$  free-free continuum. The frequency  $\nu_k$  and the corresponding luminosity  $L_k$  at which the spectral index changes, depend on the BH and stellar population masses, and also on the gas mass. Thus, the observed  $\nu_k$  and  $L_k$  provide two interrelations connecting the three masses:  $M_\bullet$ ,  $M_*$  and  $M_g$ .

- Measuring the mass of stellar population is possible only for a relatively low mass of BH  $M_\bullet \lesssim 3 \times 10^6 M_\odot$ , otherwise stellar emission is totally outshined by the BH emission.

- Line ratios are not single-valued functions of the mass ratio  $M_\bullet/M_*$ , and thus cannot serve to measure this ratio.

- The thermal dust emission in its peak around  $70 \mu\text{m}$  and the hard X-ray emission at  $\lambda \sim 2\text{--}4 \text{ \AA}$  allow us to measure masses of the stellar population and the black hole.

- Interrelations between the fluxes (luminosities) of X-ray photons with  $E \sim 3 \text{ keV}$  and submillimeter emission at  $\lambda \sim 200 \mu\text{m}$  allow to infer the gas mass in the galaxies, where the BH mass is  $M_\bullet > 10^5 M_\odot$  and the stellar population luminosity  $L_*/L_\odot < 3 \times 10^4 (M_\bullet/M_\odot)$ .

- The dependences of the ratio  $L(10 \text{ \AA})/L(1 \text{ \AA})$  vs  $L(200 \mu\text{m})$  traces the interrelation between the dust and gas masses, though they remain essentially invariant for stellar luminosities  $L_* \lesssim L_{BH}$ . In case of higher  $L_*$ , the correlations shift to higher submm luminosity emission at  $200 \mu\text{m}$ .

## 6 ACKNOWLEDGEMENTS

This work is supported by the joint RFBR-DST project (RFBR 17-52-45063). EV is grateful to the Ministry for Education and Science of the Russian Federation (grant 3.858.2017/4.6). The work by YS is done under partial support from the project 01-2018 “New Scientific Groups LPI”.

## REFERENCES

- Abramowicz, M. A., Czerny, B., Lasota, J. P., Szuszkiewicz, E., 1988, ApJ, 332, 646
- Agarwal, B., Davis, A. J., Khochfar, S., et al. 2013, MNRAS, 432, 3438
- Bell, E. F., de Jong, R. S., 2001, ApJ, 550, 212
- Bentz, M. C., Donney, K. D., Grier, C. J., et al. 2013, ApJ, 767, 149
- Bentz, M. C., Manne-Nochilas, E., 2018, ApJ, 864, 146
- Bruzual, Charlot, 2003
- Circosta, C., Vignali, C., Gilli, R., et al. 2019, A&A, 623, A172
- Compiègne, M., Verstraete, L., Jones, A., et al. , 2011, A&A, 525, A103
- Connor, T., Bañados, E., Stern, D., et al. 2020, ApJL, 884, L31
- D’Amato, Q., Gilli, R., Vignali, C., et al. 2020, arXiv:2003.08631
- Decarli, R., Walter, F., Venemans, B. P., et al. 2018, ApJ, 857, 97
- Draine, B. T., Interstellar and Intergalactic Medium
- Dwek, E., Arendt, R. G., 1992, ARA&A, 30, 11

- Ferland, G.J., Chatzikos, M., Guzmán, F. et al. 2017, *Rev. Mex. de Astron. Astrofis.*, 53, 385
- Girardi L., Bressan A., Bertelli G., Chiosi C., 2000, *A&AS*, 141, 371
- Graham, A. W., Scott, N., 2013, *ApJ*, 764, 151
- Häring, N., Rix, H. W., 2004, *ApJL*, 604, L89
- Heckman, T. H., Best, P. N., 2014, *ARA&A*, 52, 589
- Into, T., Portinari, L., 2013, *MNRAS*, 430, 2715
- Kauffmann, G., et al. 2003, *MNRAS*, 341, 33
- Kormendi, J., Ho, L. C., 2013, *ARA&A*, 51, 511
- Kubota, A., & Done, C. 2018, *MNRAS*, 480, 1247
- Latif, M. A., Ferrara, A., 2016, *PASA*, 33, 51
- Lambrides, E., Chiaberge, M., Heckman, T., et al. 2020 [arXiv:2002.00955](https://arxiv.org/abs/2002.00955)
- Lupi, A., Haardt, R. Dotti, M., 2016, *MNRAS*, 456, 2993
- Madau, P., Haardt, F., Dotti, M., 2014, *ApJ*, 784, L38
- Marconi, A., Hunt, L. K., 2003, *ApJL*, 589, L21
- Natarajan, P., 2014, *GRGr*, 46, 1702
- Natarajan, P., Pacucci, F., Ferrara, A., et al. 2017, *ApJ*, 838, 117
- Novikov, I. D., Thorne, K., 1973, in: *Black Holes*, eds. C. de Witt & B. S. de Witt, Gordon & Breach, p. 345
- Pacucci, F., Ferrara, A., Grazian, A., et al. 2016, *MNRAS*, 459, 1432
- Pacucci, F., Volonteri, M., Ferrara, A., 2015, *MNRAS*, 452, 1922
- Pezzulli, E., Valiante, R., Schneider, R., 2016, *MNRAS*, 458, 3047
- Reines, A. E., Volonteri, M., 2015, *ApJ*, 813, 72
- Salim, S., Charlot, S., Reach, A. M., et al. 2005, *ApJ*, 619, L39
- Sadowski, A., 2009, *ApJSS*, 183, 171
- Sani, E., Marconi, A., Hunt, L. K., Risaliti, G., 2011, *MNRAS*, 413, 1479
- Tanaka, T., Haiman, Z., 2009, *ApJ*, 696, 1798
- Valiante, R., Schneider, R., Volonteri, M., Omukai, K., 2016, *MNRAS*, 462, 3146
- Valiante, R., Schneider, R., Zappacosta, L., et al. 2018, *MNRAS*, 476, 407
- Vito, F., Brandt, W. N., Bauer, F. E., et al. 2019, *A&A*, 2628, L6
- Volonteri, M., 2012, *Sci?* 337, 544
- Volonteri, M., Silk, J., Dubus, G., 2015, *ApJ*, 804, 148
- Volonteri, M., Reines, A. E., 2016, *ApJ*, 820, L6
- Volonteri, M., Dubois, Y., Pichon, C., Devriendt, J., 2016, *MNRAS*, 460, 2979
- Volonteri, M., Reines, A. E., Atek, H., et al. , 2017, *ApJ*, 849, 155
- Wilms, J., Allen, A. McCray, R., 2000, *ApJ*, 542, 914
- Woo, J.-H., Schulze, A., Park, D. et al. 2013, *ApJ*, 772, 49

## APPENDIX A: INTENSITIES VERSUS METALLISITY

Increase of gas metallicity, under other conditions being equal, enhances radiative cooling and shifts thermal equilibrium to a slightly lower temperature. As a results recombination rates increase and result in a decrease of fractional ionization. This results in turn in a weakening of hydrogen recombination lines  $\propto Z^{-1/4}$ . It is demonstrated in left pan-

show that optical, infrared and submm lines of the ions of heavy metals rise nearly proportional with  $Z$ . Note that here we use the SED for a young (30 Myr) stellar population for all gas metallicity values.

## APPENDIX B: INTENSITIES VERSUS GAS MASS

When the stellar population dominates – for the Eddington luminosity it is when  $M_{\bullet}/M_{\odot} \leq 3 \times 10^{-5}(L_{\star}/L_{\odot})$ , it overwhelms the nebular emission and the metals spectral lines are uneloquent, as can be seen in Figure 10, and hardly can be used to infer the gas mass. Situation changes for  $M_{\bullet}/M_{\odot} > 3 \times 10^{-5}(L_{\star}/L_{\odot})$  with a well shaped nebular spectrum showing explicit dependence on gas mass. The most interesting feature is an approximately inversely proportional decrease of X-ray emission due to strong absorption seen at  $\lambda \sim 10\text{\AA}$ , and an approximately proportional increase of emission in submm waveband at  $\sim 200\mu\text{m}$  with growing gas mass, Figure B1.

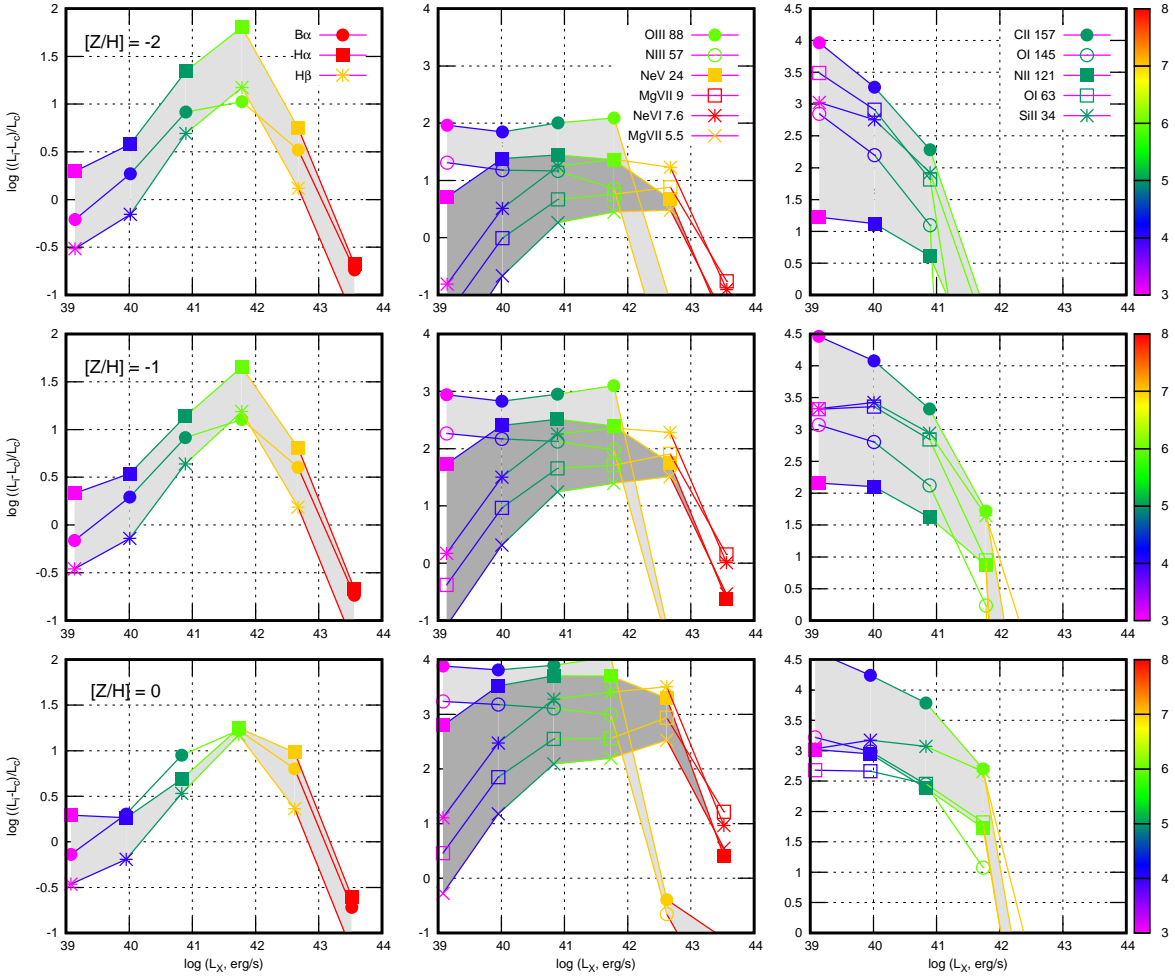


**Figure A1.** The line intensities as in Figure 7 for different gas metallicity:  $[Z/H] = -2, -1, \text{ and } 0$ , from top to bottom.

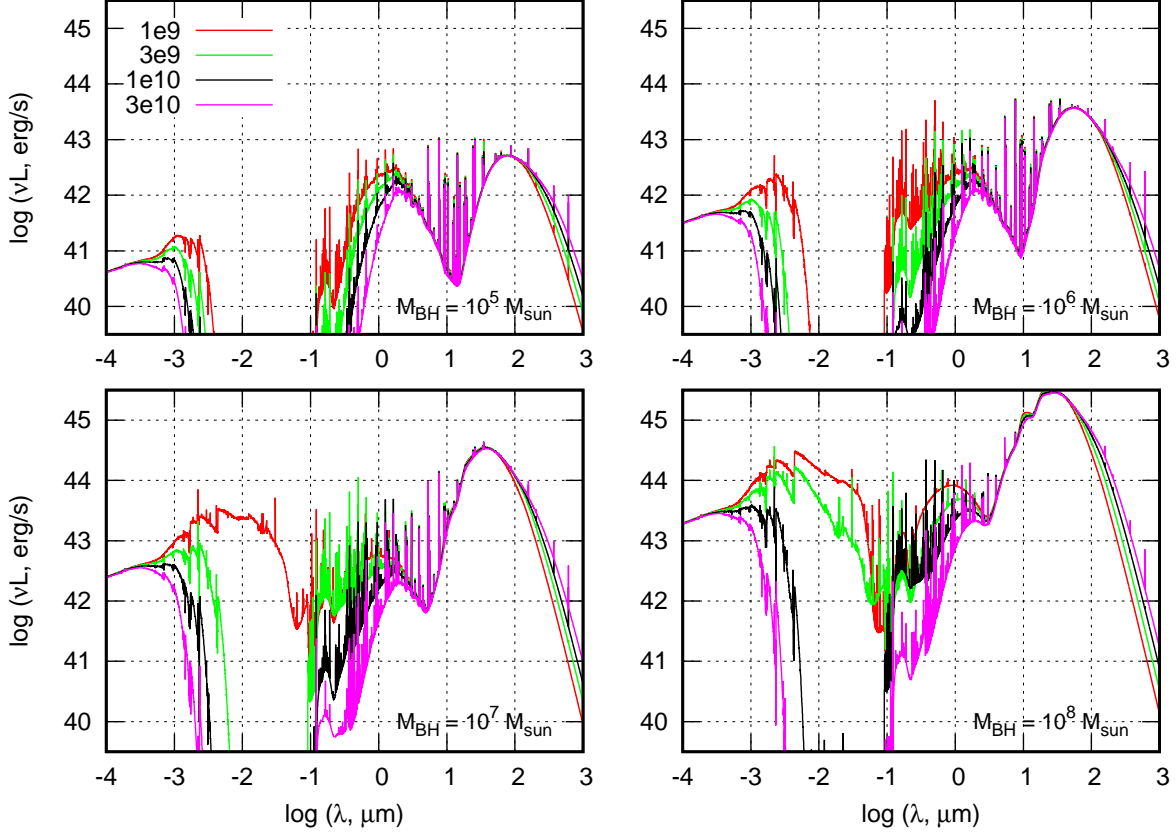


**Figure B1.** Nebular emission from gas exposed by the stellar population with bolometric luminosity  $L_* = 3 \times 10^9 L_\odot$  and the black hole with masses  $M_\bullet = 10^5, 10^6, 10^7$  and  $10^8 M_\odot$  from left top to right bottom, respectively. Different curves depict spectra of gas mass as legended; gas metallicity  $[Z]=0$ , dust mass fraction assumed as in the Milky Way  $\mathcal{D} = 0.3\zeta$ ; decrease of X-ray luminosity at  $\lambda \gtrsim 10\text{\AA}$ , and increase of nebular FIR emission  $\lambda \gtrsim 200\mu\text{m}$  with an increase of gas mass (from red to magenta lines are clearly seen). The stellar population has age 1 Gyr and solar metallicity.